

Engineering Floquet topological phases using elliptically polarized light

Ranjani Seshadri^{1,*} and Diptiman Sen^{2,†}

¹*Department of Physics, Ben-Gurion University of the Negev, Beer-Sheva 84105, Israel*

²*Centre for High Energy Physics, Indian Institute of Science, Bengaluru 560012, India*

(Dated: June 8, 2022)

We study a two-dimensional topological system driven out of equilibrium by the application of elliptically polarized light. In particular, we analyze the Bernevig-Hughes-Zhang model when it is perturbed using an elliptically polarized light of frequency Ω described in general by a vector potential $\mathbf{A}(t) = (A_{0x} \cos(\Omega t), A_{0y} \cos(\Omega t + \phi_0))$. (Linear and circular polarizations can be obtained as special cases of this general form by appropriately choosing A_{0x} , A_{0y} , and ϕ_0). Even for a fixed value of ϕ_0 , we can change the topological character of the system by changing the ratio of the x and y components of the drive. We therefore find a rich topological phase diagram as a function of A_{0x} , A_{0y} and ϕ_0 . In each of these phases, the topological invariant given by the Chern number is consistent with the number of spin-polarized states present at the edges of a nanoribbon.

I. INTRODUCTION

Topological insulators (TIs) - exotic phases of matter characterized by a gapped bulk hosting robust, conducting boundary modes - have been the talk of the town for the last several years. These could be three-dimensional systems with two-dimensional surface states, or two-dimensional systems which have one-dimensional edge modes. These materials have been studied extensively both theoretically and experimentally [1–5]. A defining feature of such systems is the existence of a bulk-boundary correspondence, i.e., a topological invariant (for example, a Chern number for two-dimensional TIs) derived from the bulk bands, defines the properties of the boundary states.

While topological materials are, by themselves, quite interesting to study, driving them out of equilibrium using a perturbation periodic in time constitutes a rapidly evolving area of research [6–23]. In particular, one can generate topological phases by driving a system which was non-topological to begin with. The underlying reason for this is that while the instantaneous Hamiltonian lies in a trivial phase, the unitary time-evolution operator over one drive cycle is topological and has eigenstates localized near the boundaries. Such phases are termed as Floquet topological systems, since one employs Floquet theory - which relies on the perfect time-periodicity of the drive - in order to analyze them.

Irradiating materials with polarized light is one of the several way of experimentally generating such Floquet topological insulators. There have been several studies which demonstrate that using circularly polarized light to drive materials can generate and/or modify topological phases [24–27]. However, to the best of our knowledge, there are relatively few works which have studied the effect of the more general case of elliptically polarized light [16, 28–31]. While the effect of using elliptically polarized

light may seem to be qualitatively similar to that of circularly polarized light in some aspects, some features are markedly different. The deviation from circular polarization introduces an anisotropy into the time-dependent model, thereby modifying the topological properties.

In this work we study the effect of tweaking the polarization of light and see how the effect changes as we vary the polarization. Elliptically polarized light can be created by superposing two linear or circularly polarized beams having a phase difference. We are interested in studying the dependence of the topological properties of a driven system on the phase of the polarized light as well as on the relative amplitudes in the two directions.

We begin in Sec. II with an overview of the Bernevig-Hughes-Zhang (BHZ) model of a two-dimensional TI and analyze the symmetries and spectrum, along with the various phases generated by tuning the parameters of the equilibrium model. This is followed in Sec. III by a brief discussion on elliptically polarised light which is then used to drive the BHZ system in Sec. IV. The topological properties of this driven system are found to depend on the driving parameters, namely, the x and y components of the oscillating vector potential and their phase difference. We find multiple topological phases which are characterized by their Chern numbers. These are reflected in the edge states of a nanoribbon of the BHZ system which is analyzed in Sec. V. Finally we conclude with a summary of the results and possible future directions in Sec. VI.

II. BERNEVIG-HUGHES-ZHANG MODEL

The equilibrium half-BHZ system [2] with mass M and spin-orbit coupling (SOC) Δ is governed by the momentum-space Hamiltonian given by

$$H = \sum_{\mathbf{k}} \begin{pmatrix} c_{\mathbf{k},\uparrow}^\dagger & c_{\mathbf{k},\downarrow}^\dagger \end{pmatrix} h(\mathbf{k}) \begin{pmatrix} c_{\mathbf{k},\uparrow} \\ c_{\mathbf{k},\downarrow} \end{pmatrix} \quad (1)$$

* ranjanis@post.bgu.ac.il

† diptiman@iisc.ac.in

where

$$h(\mathbf{k}) = (M + \gamma \cos k_x + \gamma \cos k_y)\sigma^z + \Delta(\sin k_x \sigma^x + \sin k_y \sigma^y). \quad (2)$$

Here $\sigma^{x,y,z}$ are the 2×2 Pauli matrices, and γ is the hopping amplitude which we will generally set to unity (we will also set $\hbar = 1$). This system falls under class D in the Altland-Zirnbauer classification [32] and has the following symmetries.

1. *Modified time-reversal \mathcal{T}* : While the standard time-reversal symmetry Θ is absent, the Hamiltonian in Eq. (2) has a modified time-reversal symmetry \mathcal{T} which is a product of Θ and a mirror reflection \mathcal{M}_x about the $k_x = 0$ line, i.e., $\mathcal{T}h(\mathbf{k})\mathcal{T}^{-1} = h(\mathbf{k})$ where $\mathcal{T} = \mathcal{M}_x\Theta$.
2. *Four-fold rotation \mathcal{C}_4* : $h(\mathbf{k})$ has a four-fold rotation symmetry about the z -axis, i.e., $\mathcal{C}_4 h(\mathbf{k})(\mathcal{C}_4)^{-1} = h(\mathcal{C}_4 \mathbf{k})$. The operator $\mathcal{C}_4 = e^{-i(\pi/4)\sigma^z}$ rotates the spins about the z -axis and transforms the momenta as $\mathcal{C}_4(k_x, k_y) = (k_y, -k_x)$.
3. *Particle-hole symmetry \mathcal{P}* : We see from Eq. (2) that the system has a charge conjugation or particle hole symmetry such that $\mathcal{P}h(\mathbf{k})\mathcal{P}^{-1} = -h^*(-\mathbf{k})$. This is reflected in the symmetry of the bands about the $E = 0$ plane in Fig. 1(b).

For a non-zero Δ , the spectrum is gapped, in general, except when $M = 0, \pm 2$. We calculate the Chern number

$C_{+(-)}$ for the top (bottom) band using the method prescribed in Fukui et. al. [33]. The phase-diagram for this half-BHZ system at equilibrium is shown in Fig. 1(a). Every gap closing is accompanied by a change in the Chern number. We see from the phase diagram that,

$$C_+ = \begin{cases} +1, & \text{for } -2 < M < 0, \\ -1, & \text{for } 0 < M < 2 \\ 0, & \text{for } |M| > 2. \end{cases} \quad (3)$$

In order to verify the bulk-boundary correspondence we consider an infinitely long nanoribbon having a finite width ($= N_y$ sites) in the \hat{y} direction and running parallel to the x -axis. Since the system has translation invariance along the \hat{x} direction, we take momentum k_x as a good quantum number. However, the finite width along \hat{y} breaks translation symmetry and therefore we take a finite one-dimensional chain in real space parallel to y -axis. The Hamiltonian can therefore be written as follows

$$H = h_{k_x} + \sum_{n_y} \frac{\gamma}{2} (c_{n_y, \uparrow}^\dagger c_{n_y+1, \uparrow} - c_{n, \downarrow}^\dagger c_{n_y+1, \downarrow}) - \sum_{n_y} \frac{\Delta}{2} (c_{n_y, \uparrow}^\dagger c_{n_y+1, \downarrow} - c_{n, \downarrow}^\dagger c_{n_y+1, \uparrow}) \quad (4a)$$

where h_{k_x} is a $2N_y \times 2N_y$ matrix containing the k_x -dependent terms, i.e.

$$h_{k_x} = \mathbb{I}_{N_y} \otimes \left((M + \gamma \cos k_x)\sigma^z + \Delta \sin k_x \sigma^x \right). \quad (4b)$$

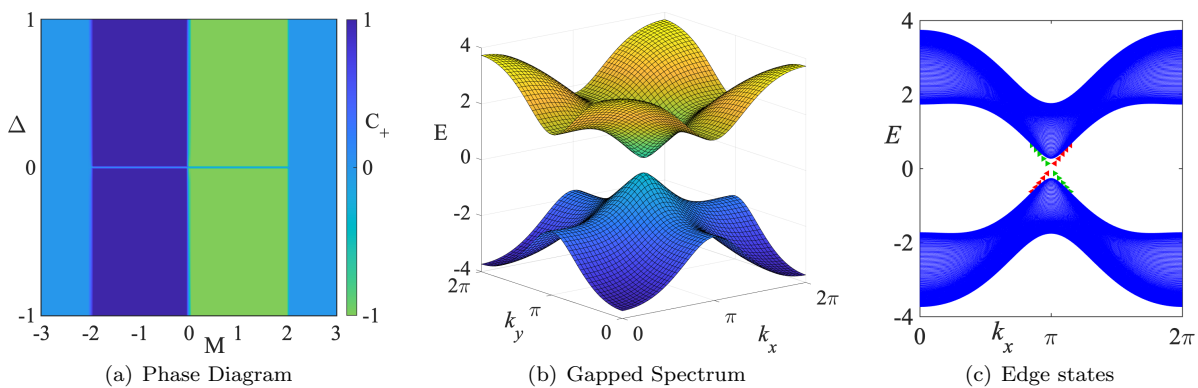


FIG. 1. (a) Trivial and topological phases of the BHZ model. The system is in a trivial phase when $|M| > 2$. The region $-2 < M < -1$ is topological with Chern number of top band $C_+ = 1$ whereas in the region $1 > M > 2$ has $C_+ = -1$. (b) The energy spectrum when $M = \sqrt{3}$, $\Delta = \sqrt{2}$ is gapped. This corresponds to the white dot in (a) which lies in the $C_+ = 1$ phase. (c) Edge state spectrum for a nanoribbon parallel to the \hat{x} direction with a finite width $N_y = 100$ sites in the \hat{y} direction. The bulk states are depicted in blue. The right (left) pointing triangles depict states with spin pointing along the $\pm \hat{x}$ directions, while the color red (green) corresponds to states localized at the bottom (top) edge of the nanoribbon.

The edge modes obtained from here are shown in Fig. 1(c). The continuum formed by the bulk states is shown

in blue. These are separated by an energy gap which host the modes localized along the edges of the ribbon

(green for top edge and red for the bottom edge). These edge states are also eigenstates of σ^x . The right and left pointing arrows correspond to states with $\sigma^x = \pm 1$ respectively. Clearly, all the right moving modes (group velocity $v_g = \partial E / \partial k_x > 0$) are localized on the bottom edge and have $\sigma^x = -1$ whereas the left movers (i.e., $v_g < 0$) lie on the top edge and have $\sigma^x = 1$.

Now that we have outlined the behavior of the equilibrium model, we perturb the system using a time-periodic optical drive. Before we discuss the properties of the driven BHZ model, we first recap the properties of polarized light and describe the form of time-dependent perturbation we use.

III. ELLIPTICALLY POLARIZED LIGHT

The most general form of the vector potential associated with elliptically polarized light is

$$\mathbf{A}(\mathbf{t}) = (A_{0x} \cos(\Omega t), A_{0y} \cos(\Omega t + \phi_0)), \quad (5)$$

where ϕ_0 is the phase difference between the x and y components. The time-dependent electric field is therefore,

$$\begin{aligned} \mathbf{E}(\mathbf{t}) &= -\frac{\partial \mathbf{A}}{\partial t} \\ &= (E_{0x} \sin(\Omega t), E_{0y} \sin(\Omega t + \phi_0)), \end{aligned} \quad (6)$$

where $E_{0x(y)} = \Omega A_{0x(y)}$. The vector potential in Eq. (5) enters the momentum-space Hamiltonian via minimal coupling, $\mathbf{k} \rightarrow \mathbf{k} + \mathbf{A}$. Therefore, the bulk Hamiltonian in Eq. (2) is modified as $h(\mathbf{k}) \rightarrow h(\mathbf{k} + \mathbf{A})$. We note that linear and circular polarization are special cases of Eq. (6). In the special case when $\phi_0 = \pm\pi/2$, we obtain elliptically polarized light with the axes of the ellipse aligned with the cardinal axes. Further, if $A_{0x} = A_{0y}$ and $\phi_0 = \pm\pi/2$, we obtain left/right circularly polarized light.

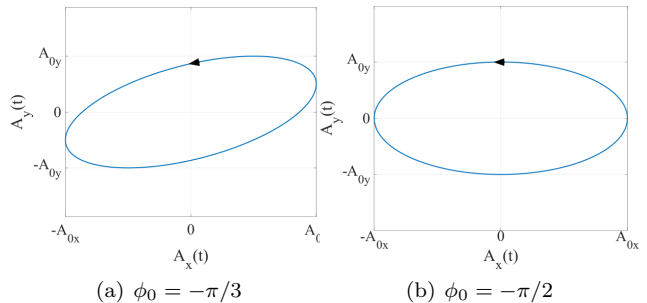


FIG. 2. The polarization ellipse for two values of phase ϕ_0 . When $\phi_0 = \pm\pi/2$, the major and minor axis of the ellipse are aligned along the cardinal axis. However, for other values of ϕ_0 the ellipse is rotated. In both these figures we have taken $A_{0x} = 0.7$ and $A_{0y} = 0.4$. The ratio of these amplitudes decides the “flatness” of the ellipse.

IV. DRIVEN TOPOLOGICAL PHASES

We now introduce a time-dependence into the problem by using a polarized light of the form given in Eq. (5). The drive frequency Ω is larger than the bandwidth of the equilibrium system. Since the drive is assumed to be perfectly periodic, we employ Floquet theory and calculate the quasienergy eigenvalues and eigenvectors by diagonalizing the Floquet operator $\mathcal{U}_T = \mathcal{T} \exp(-i \int_0^T dt H(t))$ following the discussion in App. A,

$$\mathcal{U}_T \psi_\alpha = e^{-i\epsilon_\alpha T} \psi_\alpha. \quad (7)$$

The Floquet eigenvalues ϵ_α are unique modulo $n\Omega$ where n is an integer. The primary Floquet zone where $\epsilon T \in [-\pi, \pi]$ corresponds to $n = 0$. The Floquet eigenstates ψ_α s are then used to calculate the Chern numbers. The results are shown as color plots in Fig. 3 for drive frequency $\Omega = 5$. This frequency of drive is greater than the bandwidth of the equilibrium model. Each panel corresponds to a fixed value of the phase ϕ_0 and shows the Chern number C_+ of the top band as a function of amplitudes A_{0x} and A_{0y} . We find that just by changing the ratio of the x and y amplitudes of the elliptically polarized light, we can go from one phase to another which are topologically distinct. We have chosen the parameters ($M = \sqrt{3}, \Delta = \sqrt{2}$) such that in the absence of a drive we are in a topological phase with Chern Number $C_+ = -1$, corresponding to the white dot in Fig. 1(a).

We note two symmetries in the plots in Fig. 3. First, for each value of ϕ_0 , the plots look the same when A_{0x} and A_{0y} are interchanged. Second, the plots for ϕ_0 and

$\pi - \phi_0$ look identical. We can understand these two symmetries as follows. Given the time-dependent periodic Hamiltonian with frequency Ω ,

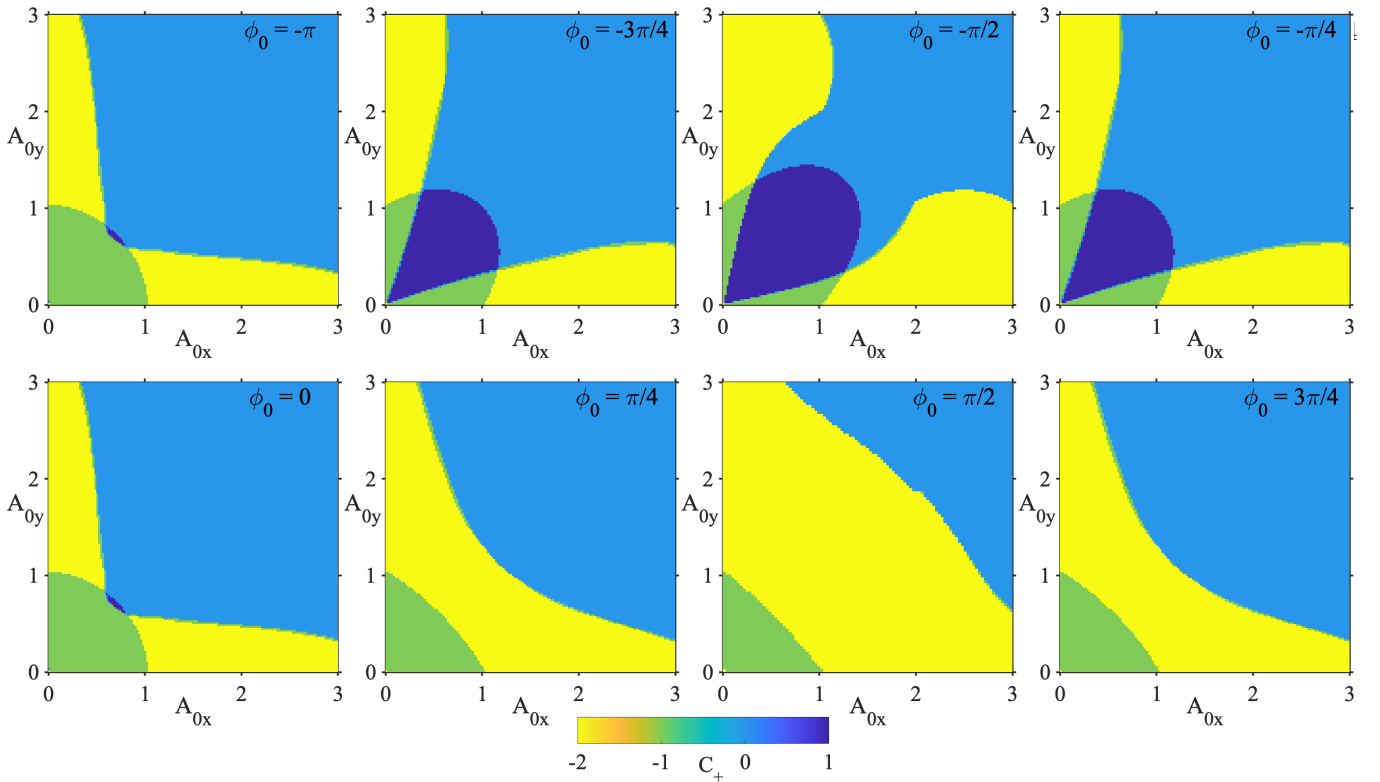


FIG. 3. Floquet Chern number C_+ of the positive quasienergy band, as a function of drive amplitudes A_{0x} and A_{0y} , for different phases ϕ_0 of the elliptically polarized light. Here we work in a parameter regime where the equilibrium system is topological with $M = \sqrt{3}$ and $\Delta = \sqrt{2}$ corresponding to the white dot marked in Fig. 1(a). The $A_{0x} = A_{0y}$ line in (c) corresponds to right-circularly polarized light. We have used $\Omega = 5$ in all panels of this figure

$$h(k_x, k_y, A_{0x}, A_{0y}, \phi_0, t) = \left[M + \cos(k_x + A_{0x} \cos(\Omega t)) + \cos(k_y + A_{0y} \cos(\Omega t + \phi_0)) \right] \sigma^z + \Delta \left[\sin(k_x + A_{0x} \cos(\Omega t)) \sigma^x + \sin(k_y + A_{0y} \cos(\Omega t + \phi_0)) \sigma^y \right], \quad (8)$$

the Floquet operator is given by

$$\mathcal{U}_T = \mathfrak{T} e^{-i \int_0^T dt h(k_x, k_y, A_{0x}, A_{0y}, \phi_0, t)}, \quad (9)$$

where \mathfrak{T} denotes time-ordering. We now observe that $\cos(\Omega t) = \cos(\Omega(T-t))$, $\cos(\Omega t + \phi_0) = \cos(\Omega(T-t) - \phi_0)$. Also, σ^x and σ^z are real whereas σ^y is imaginary. These

imply that an operator defined as

$$\mathcal{U}'_T = (\mathcal{U}_T^{-1})^* \quad (10)$$

$$= \mathfrak{T} e^{-i \int_0^T dt h'(k_x, k_y, A_{0x}, A_{0y}, \phi_0, t)}, \quad (11)$$

is the Floquet operator corresponding to a different time-dependent Hamiltonian given by

$$h'(k_x, k_y, A_{0x}, A_{0y}, \phi_0, t) = \left[M + \cos(k_x + A_{0x} \cos(\Omega t)) + \cos(k_y + A_{0y} \cos(\Omega t - \phi_0)) \right] \sigma^z + \Delta \left[\sin(k_x + A_{0x} \cos(\Omega t)) \sigma^x - \sin(k_y + A_{0y} \cos(\Omega t - \phi_0)) \sigma^y \right]. \quad (12)$$

From Eqs. (7) and (10), we see that

$$\mathcal{U}'_T \psi_\alpha^* = e^{-i \epsilon_\alpha T} \psi_\alpha^*. \quad (13)$$

Hence \mathcal{U}_T and \mathcal{U}'_T have the same quasienergies; in particular, the positive quasienergy band of \mathcal{U}_T is also the positive quasienergy band of \mathcal{U}'_T , and their eigenstates

ψ_α and ψ'_α are related as

$$\psi'_\alpha = \psi_\alpha^*. \quad (14)$$

Next, we see that the Hamiltonian h' in Eq. (12) can be transformed back to h in Eq. (8) in one of two ways. We can keep ϕ_0 unchanged, interchange $k_x \leftrightarrow k_y$ and $A_{0x} \leftrightarrow A_{0y}$, shift time $t \rightarrow t + \phi_0/\Omega$ (such a shift does

not change the eigenvalues of the Floquet operator), and, finally, perform a rotation by $\pi/2$ about the z -axis which transforms $\sigma^y \rightarrow -\sigma^x$ and $\sigma^x \rightarrow \sigma^y$. (Such a rotation which is independent of k_x, k_y unitarily transforms both the Floquet operator and its eigenstates, but does not change the Chern number defined in Eq. (15) below). Alternatively, we can change $\phi_0 \rightarrow \pi - \phi_0$ and $k_y \rightarrow -k_y$ but keep k_x, A_{0x} and A_{0y} unchanged.

Finally, we consider the expression for the Chern number in, say, the positive quasienergy band

$$C_+(A_{0x}, A_{0y}, \phi_0) = \frac{i}{2\pi} \int \int dk_x dk_y \left[\frac{\partial \psi_\alpha^\dagger}{\partial k_x} \frac{\partial \psi_\alpha}{\partial k_y} - \frac{\partial \psi_\alpha^\dagger}{\partial k_y} \frac{\partial \psi_\alpha}{\partial k_x} \right]. \quad (15)$$

We now see that the Chern number does not change if we complex conjugate ψ (as dictated by Eq. (14)) and either interchange $k_x \leftrightarrow k_y$, or change $k_y \rightarrow -k_y$ but do not change k_x . The discussion in the previous paragraph therefore shows that the Chern number $C_+(A_{0x}, A_{0y}, \phi_0)$ must remain the same if we either keep ϕ_0 unchanged and interchange $A_{0x} \leftrightarrow A_{0y}$, or we change $\phi_0 \rightarrow \pi - \phi_0$ but keep A_{0x} and A_{0y} unchanged. This explains the two symmetries which are visible in Fig. 3.

Now, according to the bulk-boundary correspondence,

the topological character of the phase is reflected in the presence/absence/number of edge states on a sample fashioned in the form a ribbon, which we describe in the following section.

V. FLOQUET EDGE MODES ON A RIBBON

The Chern numbers are directly related to the number of edge states that are present at the boundaries of a finite sample. In order to test this bulk-boundary correspondence, we consider an infinitely long nanoribbon as we did in the equilibrium case. When such a nanoribbon is irradiated with polarized light described by a vector potential in Eq. (5). This introduces a time dependence into the Hamiltonian in Eq. (4b), which we incorporate by minimal coupling and Peierls substitution i.e.,

$$\begin{aligned} k_x &\rightarrow k_x + A_{0x} \cos(\Omega t), \\ \gamma &\rightarrow \gamma e^{iA_{0y} \cos(\Omega t + \phi_0)}, \\ \text{and } \Delta &\rightarrow \Delta e^{iA_{0y} \cos(\Omega t + \phi_0)}. \end{aligned} \quad (16)$$

We then diagonalize the Floquet operator constructed using this time-dependent Hamiltonian to obtain the quasienergies which are shown as a function of momentum k_x in Fig. 4.

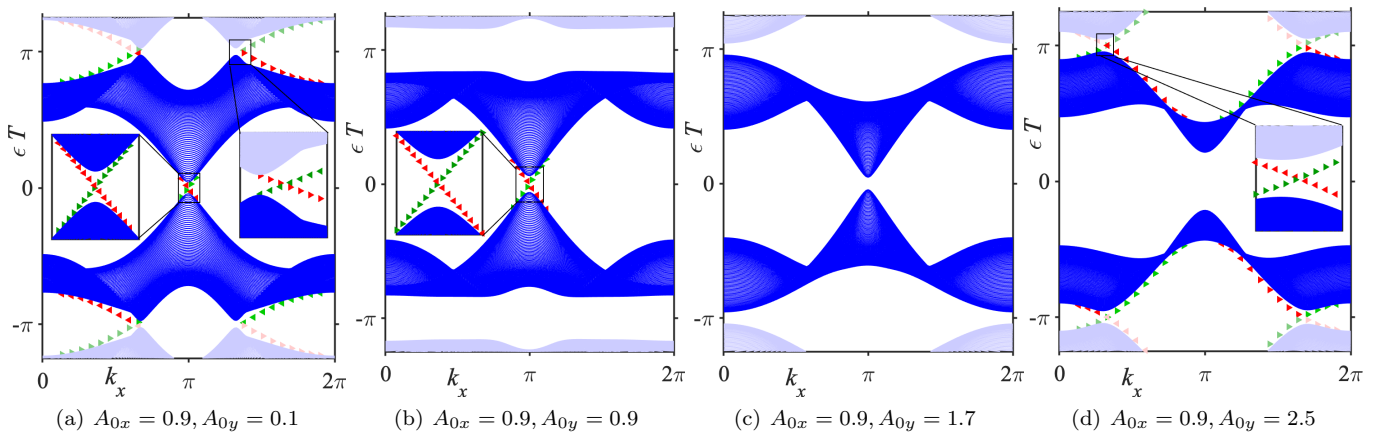


FIG. 4. Floquet edge modes on an ribbon parallel to the \hat{x} direction with a finite width $N_y = 100$ sites along the \hat{y} direction for drive frequency $\Omega = 5$ with different polarizations. These correspond to four different regions in the phase diagram shown in Fig. 2 for $\phi_0 = -\pi/2$ with Chern numbers $C_+ = -1, 1, 0$ and -2 , respectively. The right (left) pointing triangles depict states with spin pointing along the $\pm \hat{x}$ directions, while the color red (green) corresponds to the bottom (top) edge of the nanoribbon. In all the panels, the bulk states are shown in blue. The primary Floquet zone is shown in brighter color and ranges from $\epsilon T = -\pi$ to π .

While we have fixed $\phi_0 = -\pi/2$, the four panels correspond to four different pairs of values of the drive amplitudes as mentioned in the subfigure captions. All these lie in four different phases of Fig. 3(c). The continuum formed by the bulk states is shown in blue with the brighter colors denoting the primary Floquet zone (see

App. A) which corresponds to $n = 0$, i.e. $\epsilon T = -\pi$ to π . The muted colors show parts of the $n = \pm 1$ Floquet zones. These Floquet bands are separated by energy gaps which host the modes localized along the edges of the ribbon (green for top edge and red for the bottom edge). Depending upon the ratio of A_{0x} and A_{0y} , edge

modes exist at $\epsilon T = 0$ and/or $\epsilon T = \pi$. These edge states are also eigenstates of σ^x . The right and left pointing arrows correspond to states with $\sigma^x = \pm 1$ respectively. The insets in each of the panels are zoomed-in views of the edge-state dispersion.

In Fig. 4(a), we see that there are two kinds of edge states - one per edge at $\epsilon T = 0$ and two per edge at $\epsilon T = \pm\pi$. This lies in the $C_+ = -1$ phase of Fig. 3(c). On the other hand, Fig. 4(b) has only one set of edge states at $\epsilon T = 0$, which is consistent with the $C_+ = 1$ in this phase. Fig. 4(c) depicts $C_+ = 0$ phase and therefore has no edge modes, whereas Fig. 4(d) lies in the $C_+ = -2$ phase and has two sets of edge modes, both close to $\epsilon T = \pm\pi$. From this we infer that a pair of edge states at $\epsilon = 0$ correspond to $C_+ = +1$, whereas each pair of states at $\epsilon T = \pm\pi$ correspond to $C_+ = -1$. These add up along with the signs to give the total Chern number C_+ .

VI. SUMMARY AND OUTLOOK

We discuss the effects of an optical drive in the form of a general elliptically polarized light on a half-BHZ system. A range of topological phases corresponding to different Chern numbers can be generated purely by varying the driving parameters, namely, the amplitudes of the vector potential in the \hat{x} and \hat{y} directions and their phase difference ϕ_0 . We interpret this as an effect of the anisotropy that elliptically polarized light introduces into the time-dependent Hamiltonian.

Keeping the phase $\phi_0 = -\pi/2$ and varying only the ratio of the A_{0x} and A_{0y} allows us to tune in and out of topological phases even when we deviate away from the special case of circular polarization. The Chern numbers are consistent with the number of spin-polarized states localized at the two edges of an infinitely long nanoribbon with the edge states having a definite value of σ^x .

While the equilibrium model has phases with Chern numbers $0, \pm 1$, the time-dependent system driven out-of-equilibrium using an elliptically polarized light allows us to generate Floquet topological phases with higher Chern numbers as can be seen from Fig. 3. Similarly, choosing the drive parameters appropriately, the topology can even be destroyed using such an optical drive. Thus, elliptically polarized light allows us to engineer and/or modify topological phases in the half-BHZ system.

We have confined our discussion to the case of two-dimensional topological insulators with one-dimensional edge modes. However, the effect of elliptical polarization could have more significance in the context of higher-order topological systems [34]. For instance, since generating a two-dimensional second order TI with corner modes requires a perturbation that breaks the C_4 symmetry, one can expect that using elliptically polarized

light (away from the special case of circular polarization) could also achieve that [35], since the incident light (and hence the effective Floquet Hamiltonian) breaks the four-fold rotation symmetry.

ACKNOWLEDGMENTS

R.S. thanks Devendra Singh Bhakuni and Anurag Banerjee for useful discussions. D.S. thanks SERB, India for funding through Project No. JBR/2020/000043.

Appendix A: Overview of Floquet Theory

Consider a Hamiltonian which is time-dependent and is periodic in time t , i.e.,

$$H(t) = H(t + T), \quad (\text{A1})$$

where $T = 2\pi/\Omega$, Ω being the frequency. The time-dependent Schrödinger equation (setting $\hbar = 1$) is

$$\left(H(t) - i\frac{\partial}{\partial t}\right)\Psi(t) = 0. \quad (\text{A2})$$

According to Floquet theorem [36, 37], the solutions to (A2) are of the form

$$\psi_\alpha(t) = e^{-i\epsilon_\alpha t} \phi_\alpha(t), \quad (\text{A3})$$

where ϵ_α is the quasienergy which is unique modulo $n\Omega$, i.e.

$$\epsilon_\alpha \equiv \epsilon_\alpha + n\Omega, \quad n = 0, \pm 1 \pm 2 \dots \quad (\text{A4})$$

The state $\phi_\alpha(t)$ is periodic with the same time period as the Hamiltonian $H(t)$, i.e.,

$$\phi_\alpha(t) = \phi_\alpha(t + T). \quad (\text{A5})$$

The time evolution operator from any time t_1 to a later time t_2 is defined as

$$\mathcal{U}(t_2, t_1) = \mathfrak{T}e^{-i\int_{t_1}^{t_2} dt H(t)}.$$

In particular, for exactly one drive cycle, this time-evolution operator is called the Floquet operator, i.e.,

$$\mathcal{U}_T = \mathcal{U}(T, 0) = \mathfrak{T}e^{-i\int_0^T dt H(t)}. \quad (\text{A6})$$

Since $\psi(t + T) = \mathcal{U}_T \psi(t)$, from Eq. (A3),

$$\mathcal{U}_T \psi_\alpha = e^{-i\epsilon_\alpha T} \psi_\alpha. \quad (\text{A7})$$

-
- [1] M. Z. Hasan and C. L. Kane, Colloquium: Topological insulators, *Rev. Mod. Phys.* **82**, 3045 (2010).
- [2] B. A. Bernevig, T. L. Hughes, and S.-C. Zhang, Quantum spin hall effect and topological phase transition in hgte quantum wells, *Science* **314**, 1757 (2006), <https://science.sciencemag.org/content/314/5806/1757.full.pdf>.
- [3] J. E. Moore, The birth of topological insulators, *Nature* **464**, 194 (2010).
- [4] J. E. Moore and L. Balents, Topological invariants of time-reversal-invariant band structures, *Phys. Rev. B* **75**, 121306 (2007).
- [5] L. Fu, C. L. Kane, and E. J. Mele, Topological insulators in three dimensions, *Phys. Rev. Lett.* **98**, 106803 (2007).
- [6] T. Kitagawa, E. Berg, M. Rudner, and E. Demler, Topological characterization of periodically driven quantum systems, *Phys. Rev. B* **82**, 235114 (2010).
- [7] T. Kitagawa, T. Oka, A. Brataas, L. Fu, and E. Demler, Transport properties of nonequilibrium systems under the application of light: Photoinduced quantum hall insulators without landau levels, *Phys. Rev. B* **84**, 235108 (2011).
- [8] T. Oka and H. Aoki, Photovoltaic hall effect in graphene, *Phys. Rev. B* **79**, 081406 (2009).
- [9] Z. Gu, H. A. Fertig, D. P. Arovas, and A. Auerbach, Floquet spectrum and transport through an irradiated graphene ribbon, *Phys. Rev. Lett.* **107**, 216601 (2011).
- [10] N. H. Lindner, G. Refael, and V. Galitski, Floquet topological insulator in semiconductor quantum wells, *Nature Physics* **7**, 490 (2011).
- [11] E. Suárez Morell and L. E. F. Foa Torres, Radiation effects on the electronic properties of bilayer graphene, *Phys. Rev. B* **86**, 125449 (2012).
- [12] A. Kundu, H. A. Fertig, and B. Seradjeh, Effective theory of floquet topological transitions, *Phys. Rev. Lett.* **113**, 236803 (2014).
- [13] B. Dóra, J. Cayssol, F. Simon, and R. Moessner, Optically engineering the topological properties of a spin hall insulator, *Phys. Rev. Lett.* **108**, 056602 (2012).
- [14] M. Thakurathi, A. A. Patel, D. Sen, and A. Dutta, Floquet generation of majorana end modes and topological invariants, *Phys. Rev. B* **88**, 155133 (2013).
- [15] Y. T. Katan and D. Podolsky, Modulated floquet topological insulators, *Phys. Rev. Lett.* **110**, 016802 (2013).
- [16] H.-X. Zhu, T.-T. Wang, J.-S. Gao, S. Li, Y.-J. Sun, and G.-L. Liu, Floquet topological insulator in the BHZ model with the polarized optical field, *Chinese Physics Letters* **31**, 030503 (2014).
- [17] M. S. Rudner, N. H. Lindner, E. Berg, and M. Levin, Anomalous edge states and the bulk-edge correspondence for periodically driven two-dimensional systems, *Phys. Rev. X* **3**, 031005 (2013).
- [18] F. Nathan and M. S. Rudner, Topological singularities and the general classification of floquet-bloch systems, *New Journal of Physics* **17**, 125014 (2015).
- [19] D. Carpentier, P. Delplace, M. Fruchart, and K. Gawędzki, Topological index for periodically driven time-reversal invariant 2d systems, *Phys. Rev. Lett.* **114**, 106806 (2015).
- [20] T.-S. Xiong, J. Gong, and J.-H. An, Towards large-chern-number topological phases by periodic quenching, *Phys. Rev. B* **93**, 184306 (2016).
- [21] M. Thakurathi, D. Loss, and J. Klinovaja, Floquet majorana fermions and parafermions in driven rashba nanowires, *Phys. Rev. B* **95**, 155407 (2017).
- [22] B. Mukherjee, P. Mohan, D. Sen, and K. Sengupta, Low-frequency phase diagram of irradiated graphene and a periodically driven spin- $\frac{1}{2}$ xy chain, *Phys. Rev. B* **97**, 205415 (2018).
- [23] L. Zhou and J. Gong, Recipe for creating an arbitrary number of floquet chiral edge states, *Phys. Rev. B* **97**, 245430 (2018).
- [24] Q. Chen, L. Du, and G. A. Fiete, Floquet band structure of a semi-dirac system, *Phys. Rev. B* **97**, 035422 (2018).
- [25] C. Dutreix, E. A. Stepanov, and M. I. Katsnelson, Laser-induced topological transitions in phosphorene with inversion symmetry, *Phys. Rev. B* **93**, 241404 (2016).
- [26] P. M. Perez-Piskunow, G. Usaj, C. A. Balseiro, and L. E. F. F. Torres, Floquet chiral edge states in graphene, *Phys. Rev. B* **89**, 121401 (2014).
- [27] J. W. McIver, B. Schulte, F.-U. Stein, T. Matsuyama, G. Jotzu, G. Meier, and A. Cavalleri, Light-induced anomalous hall effect in graphene, *Nature Physics* **16**, 38 (2020).
- [28] K. Kitayama, Y. Tanaka, M. Ogata, and M. Mochizuki, Floquet theory of photoinduced topological phase transitions in the organic salt α -(bedt-ttf) $_2$ i $_3$ irradiated with elliptically polarized light, *Journal of the Physical Society of Japan* **90**, 104705 (2021), <https://doi.org/10.7566/JPSJ.90.104705>.
- [29] D. Baykusheva, A. Chacón, J. Lu, T. P. Bailey, J. A. Sobota, H. Soifer, P. S. Kirchmann, C. Rotundu, C. Uher, T. F. Heinz, D. A. Reis, and S. Ghimire, All-optical probe of three-dimensional topological insulators based on high-harmonic generation by circularly polarized laser fields, *Nano Letters* **21**, 8970 (2021), pMID: 34676752, <https://doi.org/10.1021/acs.nanolett.1c02145>.
- [30] H. Chnafa, M. Mekkaoui, A. Jellal, and A. Bahaoui, Effect of strain on band engineering in gapped graphene, *The European Physical Journal B* **94**, 39 (2021).
- [31] A. Díaz-Fernández, Inducing anisotropies in dirac fermions by periodic driving, *Journal of Physics: Condensed Matter* **32**, 495501 (2020).
- [32] A. Altland and M. R. Zirnbauer, Nonstandard symmetry classes in mesoscopic normal-superconducting hybrid structures, *Phys. Rev. B* **55**, 1142 (1997).
- [33] T. Fukui, Y. Hatsugai, and H. Suzuki, Chern numbers in discretized brillouin zone: Efficient method of computing (spin) hall conductances, *Journal of the Physical Society of Japan* **74**, 1674 (2005).
- [34] R. Seshadri, A. Dutta, and D. Sen, Generating a second-order topological insulator with multiple corner states by periodic driving, *Phys. Rev. B* **100**, 115403 (2019).
- [35] Z. Ning, B. Fu, D.-H. Xu, and R. Wang, Tailoring quadrupole topological insulators with periodic driving and disorder (2022).
- [36] G. Floquet, On linear differential equations with periodic coefficients, *Scientific annals of the Ecole Normale Supérieure 2nd series*, **12**, 47 (1883).
- [37] M. Holthaus, Floquet engineering with quasienergy bands of periodically driven optical lattices, *Journal of Physics B: Atomic, Molecular and Optical Physics* **49**, 013001 (2015).